World Academy of Science, Engineering and Technology
International Journal of Electrical and Computer Engineering
Vol:16, No:12, 2022

Supervisory Control for Induction Machine with a Modified Star/Delta Switch in Fluid Transportation

O. S. Ebrahim, K. O. Shawky, M. A. Badr, P. K. Jain

***Abstract*—**This paper proposes an intelligent, supervisory, hysteresis liquid-level control with three-state energy saving mode (ESM) for induction motor (IM) in fluid transportation system (FTS) including storage tank. The IM pump drive comprises a modified star/delta switch and hydromantic coupler. Three-state ESM is defined, along with the normal running, and named analog to the computer's ESMs as follows: Sleeping mode in which the motor runs at no load with delta stator connection, hibernate mode in which the motor runs at no load with a star connection, and motor shutdown is the third energy saver mode. Considering the motor's thermal capacity used (TCU) and grid-compatible tariff structure, a logic flow-chart is synthesized to select the motor state at no-load for best energetic cost reduction. Fuzzy-logic (FL) based availability assessment is designed and deployed on cloud, in order to provide mobilized service for the star/delta switch and highly reliable contactors. Moreover, an artificial neural network (ANN) state estimator, based on the recurrent architecture, is constructed and learned in order to provide fault-tolerant capability for the supervisory controller. Sequential test of Wald is used for sensor fault detection. Theoretical analysis, preliminary experimental testing and computer simulations are performed to demonstrate the validity and effectiveness of the proposed control system in terms of reliability, power quality and operational cost reduction with a motivation of power factor correction.

***Keywords*—**Artificial Neural Network, ANN, Contactor Health Assessment, Energy Saving Mode, Induction Machine, IM, Supervisory Control, Fluid Transportation, Fuzzy Logic, FL, cloud computing, pumped storage.

I. Introduction

THE use of cybernetic computing and information through Web has become a common approach to modern optimal control and management. Thanks to the advances of Internet of Things (IoT) technology, many social and industrial Web-based cybernetic applications are now feasible such as; medical diagnosis, information services, smart meters and billing, building and factory management, transportation control, and many other opportunities.

Fig. 1 shows generic block diagram of FTS connected to cloud-based cybernetic computing via internet. The computer center receives massive information from the plant's sensors, controllers, and users. Then, it performs extensive data manipulations and mathematical programming, considering various factors and physical constraints, in order to achieve optimal system management in terms of global impacts such as; reliability, service quality, power quality, load demand satisfaction at attractive energetic cost, sustainability, etc. Accordingly, the decisions of a localized-public (i.e., supervisory) control policy have to be linked, by way of design and objective, to these global impacts [1], [2].

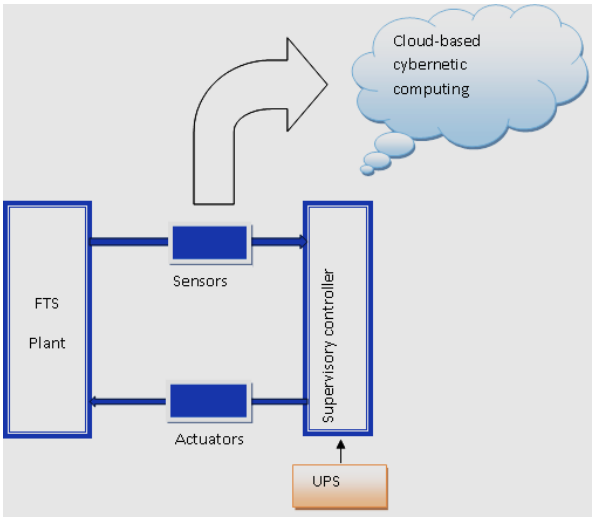

Fig. 1 Generic Blok Diagram of FTS connected to Internet

In a typical FTS, IMs driving pumps are the main consumers of electricity and most of them are squirrel cage. These motors are cheap, robust and relatively straightforward to operate. However, some precautions have to be taken due to high starting current. It can cause voltage dips and thermal overload which are problematic for the end users of the same power network and for the motor itself. Those problems can be alleviated by choosing suitable motor starting method and appropriate power supply connection [3]. Fig. 1 shows an uninterruptable power supply (UPS) feeding critical (control and protection) system components with electricity in order to make them insensitive to the electrical grid disturbances [3], [4].

More often than not, the FT process optimization requires hydraulic tank, acting as energy storage element or load time-shifter, to achieve cost reduction without violating the service quality [5]-[8]. Hourly and semi-hourly optimization periods are reported to be suitable for pumped hydro-storage in isolated power systems with large penetration of renewable energy [7].

O. S. Ebrahim, Dr., is with the Dept. of Electrical Power and Machines, Faculty of Engineering, Ain Shams University, Egypt (e-mail: osama.shawky@eng.asu.edu.eg).

K. O. Shawky is a student at the Civil Dept., Faculty of Engineering, Ain Shams University, Egypt.

M. A. Bader, Prof., is the Vice President of the Future University, Egypt (e-mail: mabadr@fue.edu.eg).

P. K. Jain, Prof., is the Director of ePOWER Research Center, Queen's University, Ontario, Canada (e-mail: parveen.jain@queensu.ca).

Fig. 2 (a) shows a hydraulic storage tank having input flow rate q_i and load flow q_0 independent of the liquid level h or head. The governing dynamic equation is given by (1) where, A is the tank cross-section area.

$$\tilde{h}(t) = \frac{1}{A}\int(q_i - q_0)dt \quad (1)$$

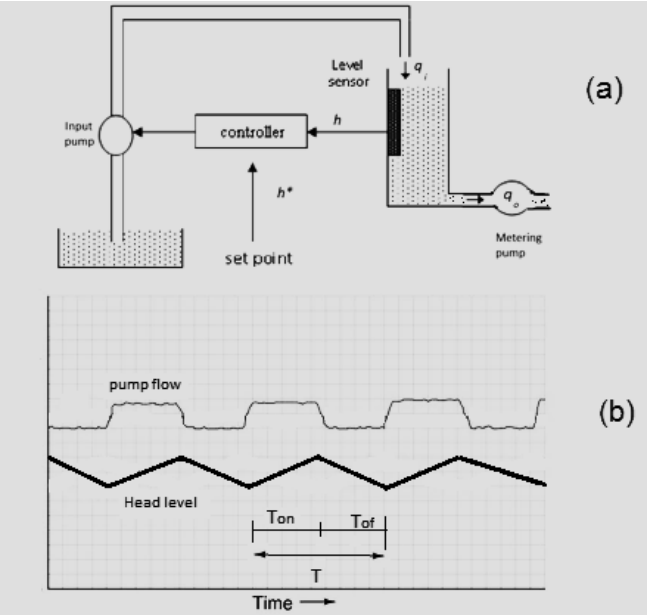

Fig. 2 Storage tank control (a) and plot of input flow and liquid-level (b)

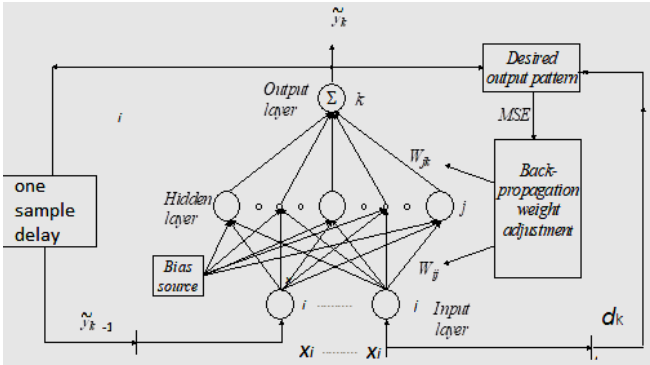

Fig. 3 Three-layer feedforward RNN

The cybernetic computer generates the head command h^* which satisfies the optimization problem over specified time interval. The supervisory controller achieves this command using on-off control or hysteresis control. Hysteretic controller offers good accuracy against unmodeled dynamics and ease of implementation. However, (1) represents a pure integrator that is sensitive to sensor noise and DC offsets [9], [10]. Therefore, online estimation of the liquid-level for fault tolerant control capability (i.e., the ability of controller to operate with satisfactory performance under sensor defects) is problematic especially; q_i and q_o are normally slow time-varying quantities. In order to overcome these difficulties, this paper exploits the full controllability and thermal capability of a motor pump drive comprising; IM, modified star/delta starter, hydromatic (fluid) coupling, centrifugal pump and a storage tank. Three motor states, during inflow off period, are distinguished and introduced. A logic flow-chart is constructed to select the best motor state for active and reactive energy cost reduction considering the motor thermal information. A FL based availability assessment is designed for the star/delta switch in order to estimate its electrical health. Besides, a recurrent neural network (RNN) state estimator is developed along with Wald's likelihood ratio test in order to provide fault-tolerant capability for the proposed control under sensor defects.

In the following sections, this control system will be illustrated and introduced. In Section II, RNN based hysteresis liquid-level controller is presented with supervision capability to detect and tolerate the sensor defects. In Section III, the IM drive is described and a closed-transition star/delta starter has been adopted considering techno-economic reasons. Three-states for the motor connection at no load have been identified and named analog to the popularly used computer's ESMs. Also, the thermal problems associated with the motor on-off operation are discussed in Section III. These problems are alleviated, in Section IV, by designing logic selector for the least expensive motor state at no-load. In Section V, a simple contactor health estimator based on FL cloud-computing is introduced as ancillary software modification to the closed-transition star/delta switch control in order to guarantee highly reliable contactors operation. Cost analysis based on preliminary testing is introduced in Section VI and the conclusion is outlined in Section VII.

II. RNN-Based Supervisory Controller

A. Hysteresis Liquid-Level Control

Hysteresis control as in Fig. 2 is a simple method of controlling the tank liquid level. The main principle is based on direct pumping of liquid such that its level or head h approximates its reference value h^* in average sense. The hysteresis block in Fig. 2 (a) compares the difference between h^* and h with a defined band, Δ, as follows

$$\begin{cases} 1 & h^* - h > \Delta \\ no\ change & -\Delta < h^* - h < \Delta \\ 0 & h^* - h < -\Delta \end{cases} \quad (2)$$

The pump on-off operation depends on whether the measured head reaches the upper or lower value of the hysteresis. Fig. 2 (b) demonstrates an example for the liquid level and input pump flow at steady state.

B. Recurrent NN Estimator

For fault-tolerant ability, the measured head h is replaced by its estimate value $\tilde{h}$ in the feedback control loop. The problem of pure integrator windup in (1) is cured by proposing full state estimator based on feedforward neural network with recurrent structure (RNN) as shown in Fig. 3. The RNN has one input layer, one hidden layer, one output layer, and biasing source. The input and output layer neurons are dictated by the number of respective signals and the hidden layer neurons with sigmoid

activation function. The synthesized RNN configuration has noise immunity and dynamic processing ability. Since the number of input neurons exceeds what is necessary to determine the output pattern, i.e. over-determined or redundant NN, it can work after training with one (or two) of its input neurons inhabited. This is similar to the case if one (or two) of the plant sensors is defected.

The fault-tolerant ability of the proposed RNN state estimator has the potential to improve the overall availability of the sensing elements. To demonstrate this, we assume that q_o, q_i, and h sensors have availability A of 80% each. The resultant availability of a RNN estimator, trained with one out of three sensors defected, will be $[1-(1-A_1A_2)(1-A_3A_2)(1-A_1A_3)] = 1-0.36*0.36*0.36 = 95.3344$ %. Furthermore, if the load flow q_o is dependent variable or its profile is known, the RNN can be trained as a best fit estimator with two sensors defected, i.e., of two out of three sensors, which increases the overall availability to $[1-(1-A_1)(1-A_2)(1-A_3)] = 1-0.2*0.2*0.2 = 99.2$ %. Here, we assume that the availability of microprocessor-based data acquisition card = 100% and the availability A = 1-failure rate.

We consider that the RNN is being trained. The training data comprise q_o, q_i, and h measurements information as input as well as desired pattern while, their corresponding estimates as output pattern. We consider that the network is being trained by the input pattern n, the weights and biases of the network are updated using the back-propagation technique to minimize the network performance function. A common performance function for the feedforward networks is the mean squared error, MSE:

$$MSE = \frac{1}{Q}\sum_{k=1}^{Q}(d_k^n - \widetilde{y_k^n})^2 \tag{3}$$

where $\widetilde{y_k^n}$ = output of the k^{th} neuron in the output layer, d_k^n corresponding desired output, and Q = dimension of the output vector (in our case Q = 3). The weights of the neurons are altered to minimize the value of MSE by gradient descent method. The weight update equation is then given as

$$W_{ij}(l+1) = W_{ij}(l) - \eta\frac{\partial MSE}{\partial W_{ij}(l)}. \tag{4}$$

where η = learning rate, $W_{ij}(l+1)$ = new weight between i^{th} and j^{th} neurons, and $W_{ij}(l)$ = corresponding old weight. The weights are iteratively updated and a momentum term $\beta[W_{ij}(l+1) - W_{ij}(l)]$ is usually added to the right hand side of (4), where β is a small value, in order to improve training performance [11], [12].

C. Data Conditioning and Fault Detection

For RNN training, measurement sets of tank variables shall be collected online during periodic phases of data acquisition. An averaged signal for each channel is computed and considered as a reference pattern. Cross correlation between coefficients of single samples and the averaged pattern are calculated. The samples with very low correlation coefficients are discarded. Fig. 4 (a) demonstrates simulated time response (using MATLAB/Simulink) of RNN based estimator for the pump outflow during training, testing, and validation phases using input signal with white noise. Fig. 4 (b) shows the samples autocorrelation-error curve and the corresponding level of confidence.

The confidence limit is similarly determined for sensor fault detection using Wald's likelihood ratio test. The method is based on choosing between two hypothesis H_0 (normal behavior) and H_1 (abnormal behavior) according to signal signature [13]. For each error signal E_k(t), we define $P(E_k^J/H_o)$ and $P(E_k^J/H_1)$ as a priori density probability where E_k^J is a vector of J samples of the signal E_k(t). The likelihood ratio is given by

$$\gamma_k = \frac{P(E_k^J/H_o)}{P(E_k^J/H_1)} = \prod_{i=1}^{J}\frac{P(E_k^i/H_o)}{P(E_k^i/H_1)} \tag{5}$$

Then the formulation of Wald's test is given by (6):

$$\begin{cases} normal & A > \gamma_k \\ no\ decision & A < \gamma_k < B \\ abnormal & B < \gamma_k \end{cases} \tag{6}$$

where A = $P_{MF}/(1-P_{RA})$ and B = $(1-P_{MF})/P_{RA}$ with P_{MF} is the probability to miss faulty measurement and P_{RA} is the probability of wrong alarm.

Wald's test for sensor fault detection can be formulated in terms of significant deviation of the reference mean value μ assuming, $P(E_k^J/H_o)$ and $P(E_k^J/H_1)$ are Gaussian:

$$\begin{cases} normal & \sum_{i=1}^{J} V_i < T_o \\ no\ decision & T_o < \sum_{i=1}^{J} V_i < T_1 \\ abnormal & \sum_{i=1}^{J} V_i > T_1 \end{cases} \tag{7}$$

The two test frontiers are as in (8):

$$T_0 = \frac{\sigma^2 lnA}{\mu_0-\mu_1} \ \ \& \ T_1 = \frac{\sigma^2 lnB}{\mu_0-\mu_1} \tag{8}$$

and

$$V_i = E_i - \frac{J(\mu_0-\mu_1)}{2} \tag{9}$$

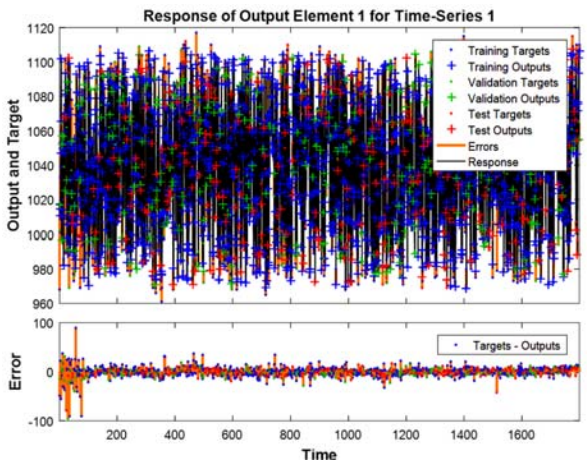

Fig. 4 (a) Time response of the RNN

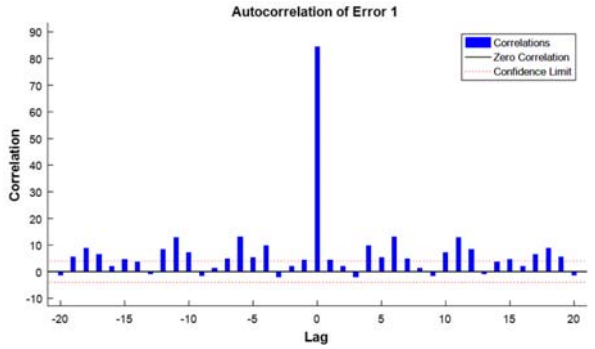

Fig. 4 (b) Autocorrelation-error curve

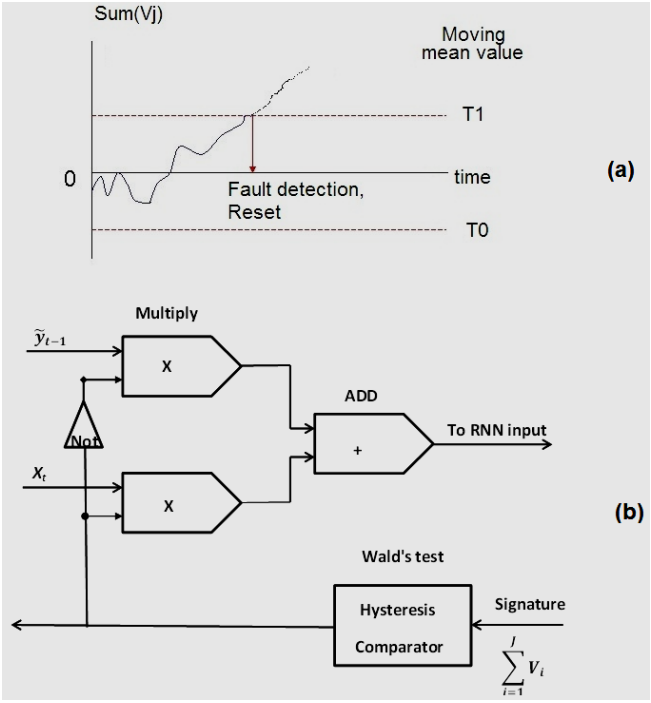

Fig. 5 Mean value, boundaries, and sensor fault detection (a) and schematic diagram of defected signal replacement (b)

Here, we assume that the mean value μ_o and the variance σ^2 are determined during learning phase when it is sure that the sensor works in normal condition and μ_1 is the increase (or decrease) in μ checking in which the sensor fault detector will be triggered as illustrated on Fig. 5 (a). Consequently, the output of Wald's test will inhabit the defected sensor signal and the corresponding input neuron will be assigned to its delayed estimate output signal as depicted schematically in Fig. 5 (b).

III. IM Drive

A. Star/Delta Starter

Recent recommendations and regulations to replace standard and high efficiency class motors with premium and super-premium ones; make IM a viable choice for FTS gross cost reduction [14]. However, higher the IM efficiency is, the higher its inrush starting current will be. The state-of-the-art electronic voltage source inverter can yield excellent dynamic speed response by varying the motor frequency but; it is not economical to be used as a starter only [11], [15]. Therefore, in applications such as on-off controlled IM pump, where dynamically varying the operating speed is less important than pump startup, stopping, and drive train isolation, the combination of electromechanical start/delta starter with hydromatic (fluid) coupling as shown in Fig. 6 represents a good fit. Such a drive is controllable and enable the motor to be rated on running rather than starting torque [15], [16].

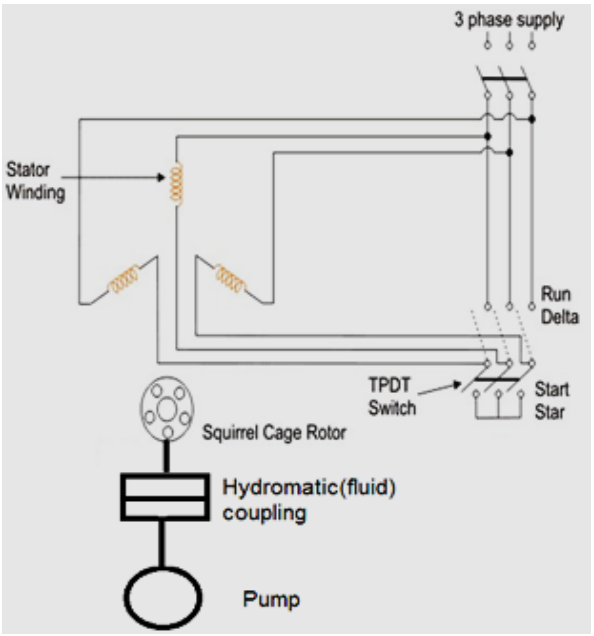

Fig. 6 IM drive with star/delta starter and hydromatic coupler

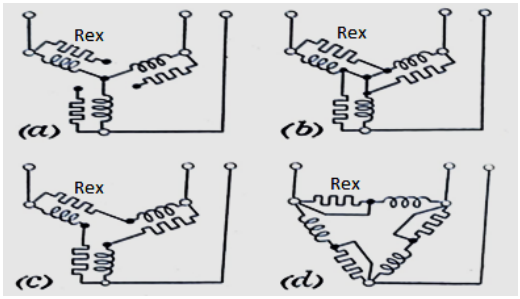

Fig. 7 Closed-transition sequence of operation [16]

The motor starts at no load with star connected stator windings, reducing the starting current and torque to one third of their nominal values. When the motor speed approaches the synchronous speed ω_1, the stator connection is changed to delta. Then, the hydromatic coupler gradually starts to load the motor by gradual coupling of the pump shaft to motor shaft. Mechanical clutches that operate too early or too suddenly will also produce severe current peaks or catastrophic pressures in the pipelines [11]. But current surges may occur for another reason even when care is taken to avoid premature operation of a change over switch. In fact, any starting method that involves a momentary disconnection of the supply main (such as; autotransformer and star/delta switch), may cause transient

current surges of a very severe nature due to remaining voltages across its terminals that decay gradually in the temporarily open circuited stator windings. When the star switch now closes in delta position, the supply voltages are reconnected to stator windings that have induced emfs of comparable size but with a relative time shift that may be anything between coincidence and opposition. In the former case, there will be a very large current surge in all phases and possibly reinforced by the magnetic saturation effect. To avoid these current surges, a star/delta starter with closed transition is used here to maintain the connection between stator and supply line, by inserting an external resistance, while changeover is made [16]. The star to delta closed-transition sequence of operation is shown in Fig. 7. The motor is switched on in star (a), resistors are paralleled with the phases (b) leaving the motor itself unaffected; the motor star point is opened (c) putting the windings in delta with series resistance; and (d) the resistors are short-circuited. The method is limited to normally delta connected motors up to rated voltage of 3000 V since, high voltage motors are usually star connected for techno-economic reasons.

B. Three-State ESM

By considering the full controllability of the proposed drive, three possible states for the motor during inflow off period (T_{off}) can be discriminated. They are named, analog to the popularly used computer's ESMs as follows:

1. Sleeping Mode

The motor is decoupled from the pump shaft and runs at no load with delta connected stator windings. The active and reactive energy consumptions are given by

$$W_{nl\Delta} \approx \frac{3V_1^2}{R_c} T_{off} \;\; \& \;\; Q_{nl\Delta} \approx \frac{3V_1^2}{X_m} T_{off} \tag{10}$$

where V_1, R_c and X_m, respectively, are the per phase nominal voltage, no load resistance and, magnetizing reactance (see Fig. 14). Thanks to the hydromatic coupler, this mode of operation achieves remarkable energy savings compared with preventing the pump flow using throttling valve.

2. Hibernate Mode

The motor runs at no load with its terminals star connected. The energy consumption will be reduced to one third of (10) assuming linear magnetic circuit, i.e.,

$$W_{nlY} \approx \frac{3(V_1/\sqrt{3})^2}{R_c} T_{off} \;\; \& \;\; Q_{nlY} \approx \frac{3(V_1/\sqrt{3})^2}{X_m} T_{off} \tag{11}$$

However, the motor-pump system in this mode takes relatively longer time to re-operate at full load than the sleeping mode.

3. Shutdown Mode

The motor is disconnected from the grid supply and consumes no active and reactive power. However, it will loss the kinetic energy stored in its moving parts $\frac{1}{2}J\omega_1^2$. For restarting, the motor will dissipate amount of energy equals $\frac{1}{2}J\omega_1^2$ as a heat in the rotor resistance r_2 and $(\frac{r_1}{r_2})\frac{1}{2}J\omega_1^2$ as a heat in the stator resistance r_1 (see the Appendix). Assuming $r_1 = r_2$, the total active and reactive energy losses associated with the shutdown decision are

$$W_{Sh.D} \approx 1.5J\omega_1^2 \;\; \& \;\; Q_{sh.D} \approx W_{Sh.D} tan(\varphi_{st}) \tag{12}$$

where, φ_{st} is the motor phase angle at starting. Here, we assume that the reactive energy in (kVARh) is measured by measuring the active energy (kWh) and its power factor.

C. Thermal Capacity Used

Basically, thermal overload protection depends on the I^2t principle and is derived from the first order thermal model in (13) [17]:

$$\frac{d\theta}{dt} = \frac{1}{\tau}(\theta_f - \theta) \tag{13}$$

where $\theta, \theta_f,$ and τ, respectively, are temperature-rise (above ambient), final temperature-rise (above ambient), and thermal time constant. The recursive temperature solution to (13) is given in (14):

$$\theta_n = \theta_{n-1} + (\theta_f - \theta_{n-1})(1 - e^{-\frac{\Delta t}{\tau}}) \tag{14}$$

where θ_n, θ_{n-1}, and Δt , respectively, are the calculated present temperature, temperature at previous time step and time step between calculations. Further, $\theta_f = (I/I_{ref})^2 T_{ref}$ where I, I_{ref}, and T_{ref}, respectively, are the motor phase current, set current reference, and set temperature rise reference. TCU is calculated based on rated motor current with an overload factor applied and expressed as a percentage of maximum temperature. The thermal protection trips when TCU reaches 100%.

Calculation of the time to reach a specified temperature θ based on load and preload temperature is given by

$$t = \tau \ln(\frac{\theta_f - \theta_o}{\theta_f - \theta}) \tag{15}$$

The advantage of using thermal protection instead of overcurrent protection is that it has thermal memory. This is critically important in the event of repetitive overload (starting) where, missing the motor thermal information could lead to numerous problems such as insulation failure. On the other hand, imposing the maximum permissible number of consecutive start/hr as a constraint in the FTS optimization problem adds difficulty and reduces the effectiveness of the solution. This is because the permissible number of consecutive cold start/hr is different from the permissible number of consecutive hot start/hr. In the followings, we will construct a logic flow chart that relax this burden up to scale it becomes useful even for the human operators.

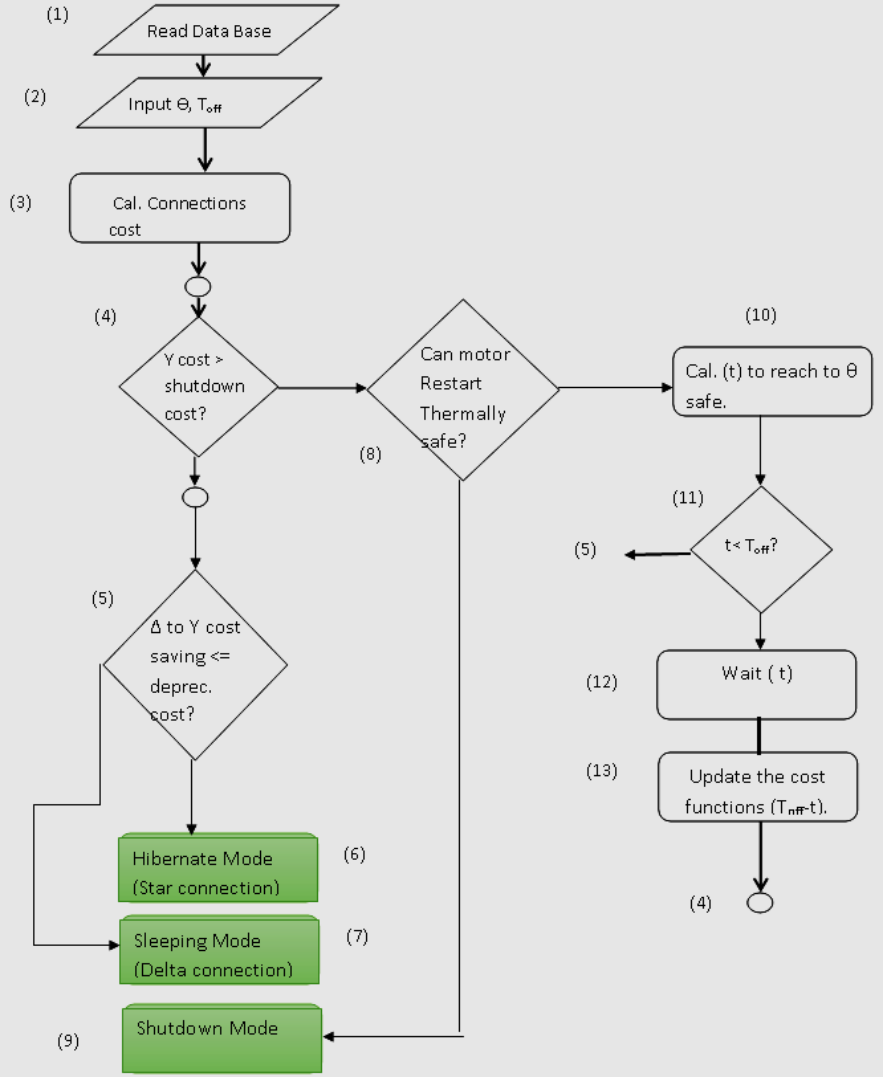

Fig. 8 Three-state ESM Logic selector

IV. Logic Flow Chart

A logic flow chart is synthesized to select the least expensive motor state during inflow off period (T_{off}), based on the following assumptions:

i) The distribution system feeding the motor and the motor branch circuit are not poor designed such that starting of an IM using star/delta starter can lead to supply interruption (i.e., comply with NEC430-52 standard).

ii) In deregulated electricity market with the suggestion of power quality market, we expect using suitable meters and tariff structure such that the customers are paying for their emission of electrical disturbances and harmonics into the distribution network. These emissions may be caused by excessive reactive power consumption during IM starting or harmonic currents generated by electronic source inverter with input diode bridge rectifier. In such a way, these customers are encouraged to install power factor correction (PFC) or harmonic filter to mitigate their power quality problems [3], [16], [18].

iii) The load profile is known, so that the variations of hysteric control period ($T = T_{on} + T_{off}$) due to operating point changes can be compensated.

The procedure consists of the following steps shown in Fig. 8.

Step1. Read the data base file. The following data must be supplied; motor thermal rates, cost of 1 kWh, cost of 1 kVARh and any power quality (PQ) indices if existing, no-load active and reactive losses.

Step2. Input the motor temperature θ and T_{off} period.

Step3. Calculate the costs of motor being delta or star connected during T_{off} from (10) and (11), cost of shutdown from (12), and any existing PQ index term, and the depreciation cost of star/delta starter. The depreciation cost is calculated based on the gross cost of star/delta starter divided by its expected number of switching operations before failure typically (500,000-1000,0000 times) or (250,000-500,000 life cycles).

Step4. If the star connection cost is greater than shutdown cost, go to step8.

Step5. If the cost difference between delta and star connections

is less than or equal to the depreciation cost, go to step7.
Step6. Change the motor connection to star (hibernate mode).
Step7. Remain the motor delta connected (sleeping mode).
Step8. If θ is greater than θ_{safe} go to step10. The safe temperature θ_{safe} is calculated using starting current ratio and the acceleration time.
Step9. Shutdown mode.
Step10. Calculate the time (t) needed to reach θ_{safe} from (15).
Step11. If (t) is less than (T_{off}) go to step12 else go to step5.
Step12. Wait time (t) to cool the motor to θ_{safe}.
Step13. Update the cost functions in terms of (T_{off}-t).
Step14. Go to step4.

A counter can be added to the mode decision blocks in order to estimate the expected life-time of the star/delta switch and the time to maintain. In addition to use of mechanically interlocked switches, these modifications have the potential to improve the starter's reliability.

V. FL Availability Assessment

Automatic star/delta switch comprises electromagnetically actuated 3-phase contactors that change the motor connection in cyclic making and breaking operations. This results in inevitable wear and tear and impacts the electrical health of the contactor due to high pressure arc produced during current cut off. On closure, the contactor may experience 5 times its rated current which can be seen as important cause of contact erosion. In addition to debris, high temperature, in the contact area, causes undesirable growing up of braze alloys. Excess of braze alloys results in rising the sides of the contact tip and reduces its thickness [19]. Since highly reliable contactors are required, studies have been carried out in order to predict the contactor failure by monitoring its operational parameters [20], [21]. In [21], a sample-data based ANN model is developed to estimate the remaining life cycles utilizing the monitored contact resistance. However, the method yields high errors and it is expensive, since accurate measurements of the contactor voltage and current are required. In order to overcome this problem, we adopt using the inverse model of [21], i.e., the contact resistance as a function of the contactor (on-off) life cycles. For simplicity and scarcity of data, a piecewise linearized model has been used here as shown in Fig. 9. The trend of the resistance variation changes with the number of life cycles. By adding a digital counter to the mode decision blocks in Fig. 8, the contact resistance variations can be determined, based on the number of contactor's life cycles, at low cost.

A FL availability assessment is designed to evaluate the contactor electrical health. The FL based computing has the advantage to handle such multivalued, nonlinear, probabilistic knowledge with more accuracy [22]. The information flow of the proposed FL availability assessment of the star/delta switch is shown in Fig. 10. The algorithm has two inputs and one output. The output membership is shown in Fig. 11 where HA, MA, and LA stand for high, medium, and low availability, respectively while the FL rules are demonstrated in Table I.

TABLE I
FL Rules

Contact resistance / Life cycles	Small life cycles	Medium life cycles	Large life cycles
Large Resistance	MA	MA	LA
Medium Resistance	HA	MA	MA
Small Resistance	HA	HA	MA

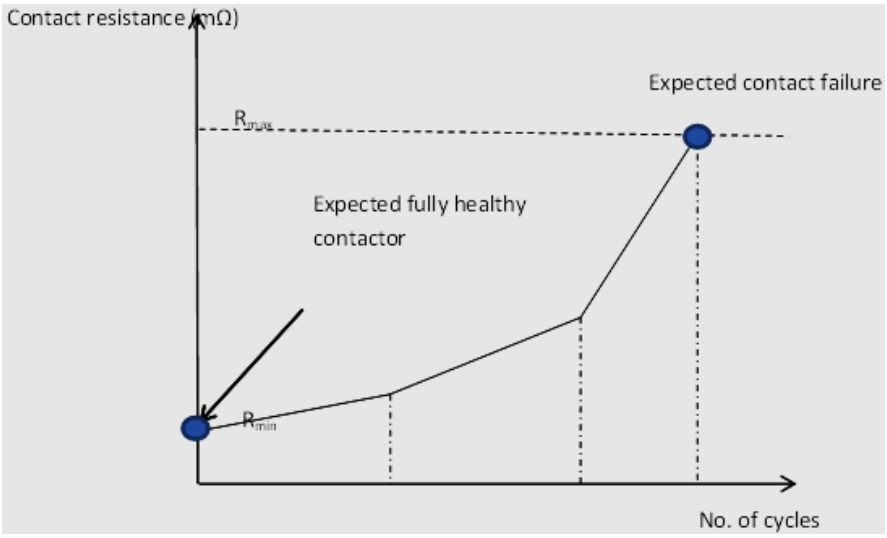

Fig. 9 Contact resistance variations with the life cycles

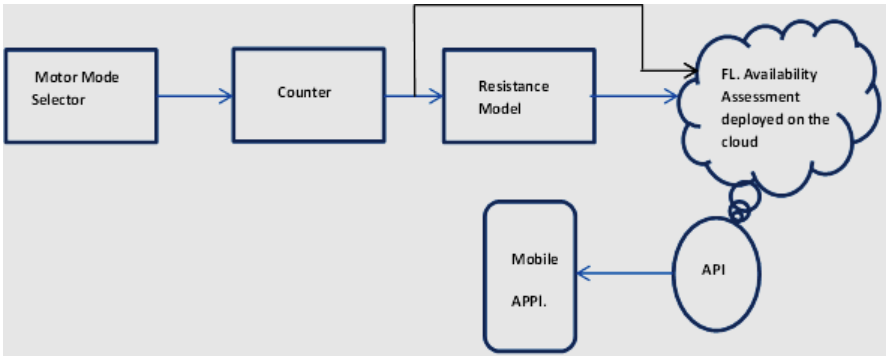

Fig. 10 Information flow

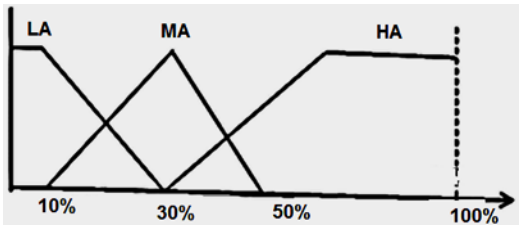

Fig. 11 Output membership function

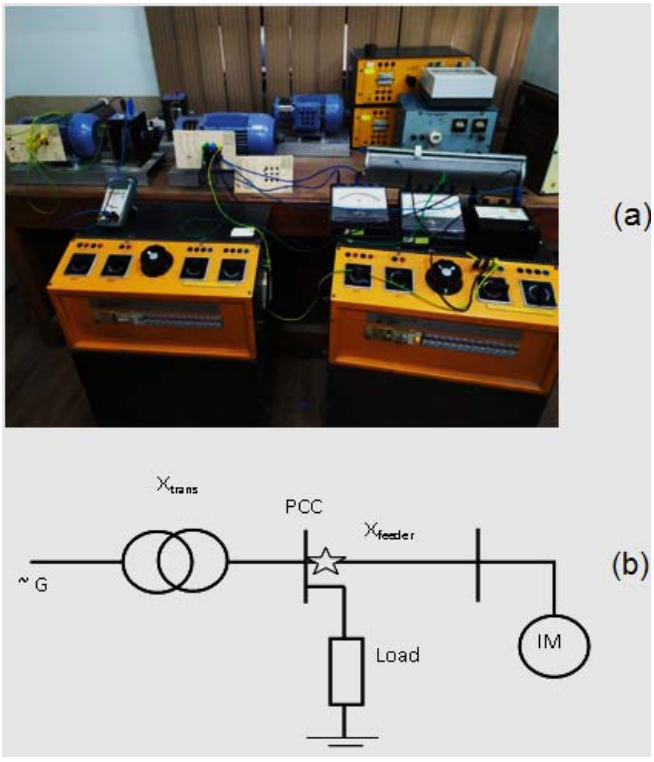

Fig. 12 IM Testing setup (a) and radial distribution system feeding the motor with a marked location for PFC (b)

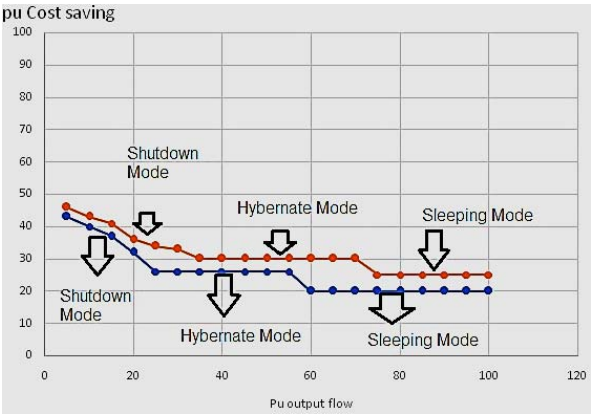

Fig. 13 Percent cost saving as a function of the % output flow

VI. Cost Analysis

Preliminary testing has been carried out on a 3-phase, 50 Hz, 4-poles, 240 V, delta-connected IM using a laboratory setup shown in Fig. 12 (a). The objective of the tests is to determine the various motor characteristics required for the logic flow ESM selector (such as; no load active and reactive power losses, per unit starting current, rotor and stator resistances, moment of inertia, motor thermal rates...etc.) considering the following conditions: ambient temp. Θ_{amb}= 30 °C, Trip temp. Θ_{Trip} = 90 °C (Y class of insulation), and safe temp. for restarting Θ_{safe} = 70 °C. Furthermore, a radial distribution system as shown in Fig. 12 (b) is assumed to supply the motor and emulated in the Lab where the reactance of the transformer and motor feeder is 4.3% of the motor KVA base, starting current = 3.2 pu, and acceleration time ≈ 4 s. The IEEE definition of voltage dip at the point of common coupling (PCC) is considered as a sudden reduction of the voltage followed by recovery after a period of time from half cycle to one minute over 10% and less than 100%. Here, we put a PQ penalty of 1% pu cost for each voltage dip occurrence due to motor shutdown and restarting that is over 10% and less than 20%.

A per unit cost analysis is performed assuming that the following parameters; C_e = 1 pu, C_Q = 0.4, and T = 30 minutes, respectively, are the cost of 1 kWh, cost of 1 kVARh, and the optimization control period. Hourly and semi-hourly optimization periods are found to be suitable for pumped hydro-storage in isolated power systems with large penetration of

renewable energy. The hysteresis control period can be predicted, compensated, and synchronized with the optimization control period using the technique presented in [23].

The cost analysis results are shown in Fig. 13, in percent at constant head, with and without PFC method installed at the upstream feeder end, respectively, indicated by the upper and lower curves. The relative cost savings are calculated with respect to the throttling cost.

The throttling power losses are emulated in the Lab. as a brake during the temperature-rise test which is carried out using two identical IMs connected to the same shaft. The first motor (the driving one) runs at rated positive sequence voltages while, the second motor is supplied by a reduced negative sequence voltages and rotates as a brake against its rotating field. In that test, the temperature-rise curves of the driven motor (brake) are determined, as well as; the throttling power losses are approximated to the input powers to the driving machine. Fig. 13 depicts noticeable effects of delta/ star transition on pu cost savings at medium flow rates. The reduction of cost savings by using restrictive tariff structure (blue curve) can be justified, from the utility point of view, by limiting the electric voltage disturbances due to repetitive starting and as a motivation for using reactive power compensation method (red curve). Consequently, with higher penalty on voltage sags due to motor starting, an efficiency optimized variable-speed pumping unit as in [11] could achieve more energetic cost reduction at low flow rates than fixed speed unit.

VII. Conclusion

This paper presented a three-state ESM and logic selector for on-off controlled IM drive with a modified star/delta switch and hydromatic coupler. The procedure implements the motor thermal information and grid-compatible tariff structure. These have the potential to alleviate burden on the FTS optimization and PQ concern. AC contactor electrical health predictor has been developed based on FL cloud computing. This has the potential to provide highly reliable contactor's operation at low cost. The scheme can be extended to wind turbines utilizing induction generators at low wind conditions. The paper also proposed a hysteresis liquid-level control with fault-tolerant ability utilizing RNN state estimator and Wald's likelihood ratio test. Investigations using computer simulations and theoretical analysis on a laboratory IM setup have been conducted and the results show validity and effectiveness of the proposed control system in terms of reliability, PQ, and cost savings.

Acknowledgment

This work is part of a research project under the supervision of Dr. O. S. Ebrahim that has been partially accepted to be published in ICSC2023 Conf. on Smart Cities, Montreal, Canada [24]. The authors would like to thank Prof. Ali Reza Bakhshai and Dr. Susan Eren at *ePOWER* research center, Queen's University, Ontario, Canada, for their encouragements and the reviewers for their constructive comments. Furthermore, the authors would like to thank the people who helped them during writing phase of this work.

Appendix

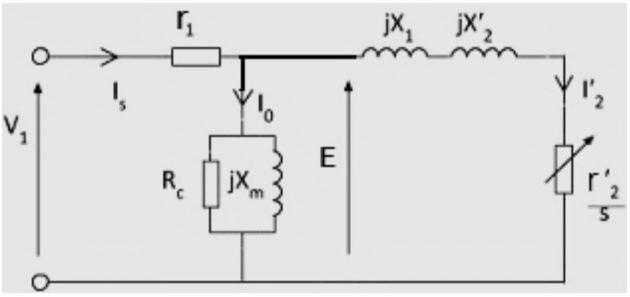

Fig. 14 An equivalent circuit for IM

The motor acceleration-time under pure inertia loads can be calculated from the dynamics of rotating mass as follows

$$M = J\frac{d\omega_r}{dt} \tag{16}$$

where *J, M,* and, ω_r respectively are the motor inertia, motor torque and rotor angular speed. From the IM equivalent circuit shown in Fig. 14, the motor torque is related to the maximum torque by

$$\frac{M}{M_m} = 2/(\frac{s}{\alpha}+\frac{\alpha}{s})\ ; \tag{17}$$

where $s = \omega_1\text{-}\omega_r/\omega_1$ and $\alpha = r_2'/(x_1+x_2')$ respectively are the slip and the slip for maximum torque. Now from (16),

$$\frac{J\omega_1}{M_m}.\frac{d}{dt}\left(\frac{\omega_r}{\omega_1}\right) = \frac{-J\omega_1}{M_m}\frac{ds}{dt} \tag{18}$$

Combining the two expressions yields

$$dt = \frac{-J\omega_1}{2M_m}(\frac{s}{\alpha}+\frac{\alpha}{s})ds \tag{19}$$

which for acceleration from standstill to slips gives

$$t = \frac{J\omega_1}{2M_m}(\frac{1-s^2}{4\alpha}+\frac{\alpha}{2}ln\frac{1}{s}) \tag{20}$$

For s = 0.1;

$$t_{acc} \approx \frac{J\omega_1}{2M_m}(\frac{0.25}{\alpha}+1.15\alpha) \tag{21}$$

Rotor Heating: The current equation can be arranged to give $I_2 = E/\sqrt{(x_1+x_2')^2+(r_s'/s)^2}$ or $I_2 \approx I_{st}/\sqrt{1+(\alpha/s)^2}$.

The rotor heat loss is $\int I_2^2 r_2 dt$ joules per phase from which (21) and (19) for a pure inertia load start is $W_{r_2} = -\frac{I_{st}^2 r_2 J\omega_1}{2\alpha M_m}\int sds = \frac{I_{st}^2 r_2 J\omega_1}{2\propto M_m}.\frac{1-s^2}{2}$. During acceleration from s = 1 to negligible slip, the rotor heat is therefore; $I_{st}^2 r_2 J\omega_1/4\alpha M_m$ joules per phase. Now the maximum torque in synchronous watts is $0.5\ E\ I_{st}$ per phase, and $\alpha = I_{st}r_2/E$; so that W_{r2} reduces quite simply to $0.5J\omega_1^2$, identical with the kinetic energy that

has been stored in the rotating parts. The heat loss W_{r2} is unavoidable and the only way to reduce this loss is to transfer part of it to an external resistance in case of slip ring motors.

Stator Heating: A heat loss comprising (r_1/r_2) W_{r2} will be consumed in the stator resistance r_1.

REFERENCES

[1] H. B. (Teddy) Pŭttgen, "R&D in our industry: where do you go from here?" *Inter. Conf. on power system technology, Powercon2004, Keynote Address, Singapore, 2004, pp.9-10.*

[2] S.M. Kaviri *et al.*, "A Supervisory Control System for Nano-grids Operating in the Stand-Alone Mode, " *IEEE Trans. on Power Electr., Volume: 36, Issue: 3, March 2021, pp. 2914–2931.*

[3] A. David, J. Maire, and M. Dessoude, "Influence of voltage dips and sags charteristics on electrical machines and drives," *the 3rd inter. Conf. on power quality end user Appl., PQA94, Netherlands, 1994, No. 1B-1.31.*

[4] S. Bagawade *et al*, "A New Discrete Four Quadrant Control Technique for Grid-Connected Full-Bridge AC–DC Converters," *IEEE Journal of Emerging and Selected Topics in Power Electr., 2021. DOI: 10.1109/JESTPE.2021.3088878.*

[5] E. Priyanka *et al*, " IoT Based monitoring and control of fluid transportation using machine learning", *ELSEVER, Computer and Electrical Engineering Journal, no. 89, 2021.*

[6] A. R. Abu'lWafa, "Industrial load management in Egypt," *the 11th proc. of inter. Assoc. of Science and Technology for Development (IASTED): Modeling, Identification, and Control, Austria, 1992, pp. 267-268.*

[7] B. D. Brown, J. A. Lopes, and M. A. Matous, "OPTIMIZATION of Pumped Storage Capacity in an Isolated Power System with Large Renewable Penetration," *IEEE TRANS. ON POWER SYSTEMS, VOL. 23, NO. 2, 2008, PP. 523-531. DOI:10.1109/TPWRS.2008.919419*.

[8] N. Mousari et al," A Real time energy management system for pumped hydro storage systems in farmhouses," *ELSEVER, Journal of energy storage, No.32,2020.*

[9] O. S. Ebrahim and P. K. Jain "LQR-based Stator Field Oriented Control for the Induction Motor Drives," the23rd IEEE Applied Power Electronic Conf. (APEC 2008), USA**,** 2008**.**

[10] O. S. Ebrahim *et al*," Application of linear quadratic regulator theory to the stator field oriented control of induction motors" *IET Electr. Power Appl., 2010, Vol. 4, Issue 8, pp. 637–646.*

[11] O. S. Ebrahim *et al*," ANN-Based Optimal Energy Control of Induction Motor in Pumping Applications," *IEEE Trans. on Energy Conversion, no.3.1, Oct. 2010.*

[12] K. Warwick, "Neural Networks for Systems and Control," *the 11th proc. of inter. Assoc. of Science and Technology for Development (IASTED): Modeling, Identification, and Control, Austria, 1992, pp. 7-10.*

[13] A. Wald, "Sequential analysis", *Dover New York, 1947.*

[14] The European commission efficiency regulations (EU) 2019/1781: For low voltage electric motors and variable speed drives.

[15] Ian Miller, "Fluid Couplings vs VFDs for High Inertia Rotating Driven Loads: A Selection Guide Reviewing the Merits of Both Options, " *Power Transmission Engineering, pp.44-46, 2017.*

[16] M. G. Say, "Alternating Current Machines", John Wiley & Sons, 5th edition, 1968.

[17] K. Smith and S. Jain, "The Necessity and Challenges of Modeling and Coordinating Microprocessor Based Thermal Overload Functions for Device protection," *The 70 Ann. Conf. On Protective Relay Engineers (CPRE), 2017.*

[18] O. S. Ebrahim; P. K. Jain; G. Nishith, " Digital State Control with Preview for a Shunt Active Filter Having the Function of Active Rectifier", *The 33rd Ann. Conf. of the IEEE Industrial Electronics Society* (IECON'07), 2007, Taiwan.

[19] P. J. Freeman, "Electric Power Transmission and Distribution," *Harrap publishing, 1974.*

[20] S. Kumari *et al*, "Reliability Estimation of Distribution Components-Contactors," *IEEE PES Asia Pacific power and Energy Conf.,2016.*

[21] S. Abirami *et al*," AC Contactor Electrical Health Estimator Model, " *IOP Materials Science and Engineering,2021.*

[22] C. Earl, "The Fuzzy Systems Handbook," *1994.*

[23] W. Stefanuti and P. Mattavelli,"Fully Digital Hysteresis Modulation with Switching Time Prediction," *IEEE Trans. On Ind. Appl., Vol. 42, No. 3, 2006 pp.763-769.*

[24] O. S. Ebrahim, K. O. Shawky, and, M. O. S. Ebrahim, " Supervisory Controller with Three-State Energy Saving Mode for Induction Motor in Fluid Transportation," accepted in ICSC23 Conf. on smart cities, Montreal, Canada, 2023, Paper Code: 23CA050133.

Osama S. Ebrahim received his BSc (Hons), MSc, and PhD degrees from Ain Shams University, Egypt, in 1993, 1998 and 2004 respectively. Since 2005, he has been Assistant Professor in the Electrical Power and Machines Department, Ain Shams University, and has served as a consultant engineer for the Electrical and Mechanical Research Institute, National Water Research Center, Egypt, where he provides scientific guidance in developing energy efficient and environmentally friendly variable speed pumping units. He has pursued research activities as a postdoctoral fellow at the Centre for Energy and Power Electronics Research (ePOWER), Queen's University, Canada, in 2006 and since 2008, with grant funding from the Ontario Ministry of Research and Innovation. Dr. Ebrahim is a member of IEEE and of the Egyptian Syndicate of Engineering. He was a Treasurer of the IEEE Kingston Section, Canada. His research interests include modern control theories and their digital applications to power electronic converters, FACT/s applications to power systems, sensorless motor drives, wind alternators and solar PV systems. Since 2011, Dr. O. S. Ebrahim was with the Faculty of Engineering, Ain Shams University, Egypt, continuing his research work in the area of high performance, efficient and, low cost electrical machines and energy systems.

Kareem O. Shawky is a student at the Civil Dept., Faculty of Engineering, Ain Shams University, Egypt. His research interest includes smart cities, building and hydro storage systems design, traffic management and control and intelligent cloud computing.

Mohamed A. Badr received the BSc (Hons.) degree from Cairo University, Egypt, MSc degree from Ain-Shams University, Egypt, MASc and PhD degrees from University of Saskatchewan, Canada in 1965, 1969, 1971, and 1974, respectively. He is a Professor in the Electrical Power and Machines Department, Ain-Shams University since 1986. Currently, he is a chairman in the Egyptian Supreme Council for promoting faculty staff members to higher ranks and Dean of Faculty of Engineering and Technology, Future University, Egypt. Since 2020 he became the Vice Prisendent of the future university, Egypt. Dr. Badr has a considerable contribution in developing the electrical and environmental engineering in Egypt and Saudi Arabia where he directed many conferences, workshops, consultant units and held various teaching positions.

Dr. Badr is awarded the Egyptian State Encouraging Award in Engineering Sciences in 1997 and nominated for the UNESCO science prize for outstanding contribution to the scientific development of a member state or region. He is also obtained the Egyptian State Award for Scientific Superiority in Engineering Sciences in 2004. His domain of research activities in the electrical power and machine applications includes interdisciplinary varieties and he published more than 150 conference and Journal papers and three scientific books.

Praveen K. Jain (S'86, M'88, SM'91, F'02) received a BE (Hons.) degree from the University of Allahabad, India, and MASc and PhD degrees from the University of Toronto, Canada, in 1980, 1984, and 1987, respectively, all in electrical engineering.

Presently, he is a Professor and Tier-1 Canada Research Chair in Power Electronics at Queen's University in Kingston, Ontario, Canada. He is also the founding Director of the Queen's Centre for Energy and Power Electronics Research (ePOWER).

From 1994 to 2000, Dr. Jain was a Professor at Concordia University, Montreal, Canada, where was engaged in teaching and research in the field of power electronics. Prior to this (1989-1994) he was a Technical Advisor with the Power Group, Nortel Networks, Ottawa, Canada, where he was providing

guidance for research and development of advanced power technologies for telecommunications. During 1987-1989, he was with Canadian Astronautics Ltd., Ottawa, Canada, where he played a key role in the design and development of high frequency power conversion equipments for the Space Station Freedom. He was a design engineer and production engineer at Brown Boveri Company and Crompton Greaves Ltd., India, respectively during the period of 1980-1981. He also has considerable consulting experience with the industry including Astec, Ballard, General Electric, Intel and Nortel.

Dr. Jain has attracted over $20M funding to conduct research and establish the state-of-the-art Energy and Power Electronics Applied Research Laboratory (ePEARL) at Queen's University. He has also supervised over 75 research engineers, postdoctoral fellows and graduate students. He has considerable experience in transferring technology from university lab to practical product designs. He secured over $35M venture funding to found CHiL Semiconductor to design and market mixed analog/digital semiconductor chip products. Dr. Jain has published over 375 publications including 40 patents in the area of power electronics. Dr. Jain is a Fellow of the Institute of Electrical and Electronics Engineering (FIEEE), a Fellow of the Engineering Institute of Canada (FEIC) and a Fellow of the Canadian Academy of Engineering (FCAE). He is also the recipient of 2004 Engineering Medal (R&D) of the Professional Engineers of Ontario. He is an Associate Editor of IEEE Transactions on Power Electronics, and KIPE Journal of Power Electronics. Recently, Dr. Jain has been awarded the 2021 IEEE Medal in Power Engineering.